Check for updates

Revealing anisotropy and thickness dependence of Raman spectra for SnS flakes†

Mingling Li,[a] Yiming Wu, [ID][a] Taishen Li,[a] Yulin Chen, [ID][a] Huaiyi Ding,[a] Yue Lin,[a] Nan Pan[abc] and Xiaoping Wang*[abc]

In this work, we have successfully synthesized SnS flakes with different thicknesses and systematically investigated their polarization-dependent Raman properties. It is found that the different Raman mode of SnS shows distinctly anisotropic thickness dependence. For B_{3g} mode, the polar plot of Raman intensities is insensitive to the flake thickness. However, the behavior of A_g mode is entirely different. Under parallel polarization configuration, with decreasing the flake thickness, the maximum Raman intensity of A_g mode changes from the armchair direction to the zigzag direction with 514.5 nm excitation. The results can be understood by the complex Raman tensor owing to the large absorption of SnS. Moreover, under the perpendicular polarization configuration, the Raman intensity of A_g mode along 45° direction becomes apparently different from that along 135° direction. Our finding not only deepens the understanding of anisotropic Raman properties of SnS but also provides inspiration for further studies on the other 2D IV–VI materials.

Introduction

SnS is an important member of the IV–VI two dimensional materials belonging to the space group D_{2h}^{16}.[1–3] Like other 2D materials, the in-plane S and Sn atoms are connected by covalent bonds, while the out-plane layers are connected by van der Waals interaction.[1,4] However, the existed electron lone pairs (*i.e.* Sn^{2+} $5s^2$) can enhance the interlayer interaction and make it become a distorted NaCl type structure.[5] SnS is also an earth-abundant,[6] stable[7] and non-toxic[8] material. Its large absorption coefficient ($\sim 10^5$ cm^{-1}),[9,10] as well as the predicted high carrier mobility,[7] renders it a great of potential applications in opto-electronic and electronic devices.[2,4,11–18] Moreover, similar to the black phosphorous (BP) with puckered honey-comb crystal structure, SnS also possesses anisotropic electronic,[19,20] thermoelectric,[21–23] piezoelectric[24] and optical[25,26] properties. Given the strongly anisotropic properties of SnS, the SnS–SnS$_x$Se$_{1-x}$ core–shell heterostructure with anisotropic photoresponse and

the SnS-based photodetector with highly anisotropic performance of near-infrared have been achieved.[27,28] Additionally, the anisotropic photoresponse properties of SnS can be significantly improved by combining with the plasmon enhancement provided by various metallic nanoparticles.[28–30] The anisotropic Raman property of SnS has also been observed and interpreted by Raman tensor theory.[25] Like BP,[31,32] the behavior can further be used to *in situ* identify the crystalline orientation to perform the anisotropic electrical and thermoelectrical measurement.[20,25] However, similar to that observed in BP,[33–38] the strong absorption of SnS would inevitably lead to complex elements in the Raman tensor and therefore change the anisotropic Raman properties with the thickness. However, the dependence of anisotropic behavior of SnS on the thickness has been overlooked. In this regard, it is interesting and imperative to investigate the anisotropic Raman properties of SnS flakes as well as its thickness dependence. However, to the best of our knowledge, there is no systematically study so far about this content, especially in-depth study on the complex Raman tensor elements.

In this work, we have successfully synthesized SnS flakes with different thicknesses by physical vapor deposition (PVD) method. We then systematically investigated the polarization-dependent Raman properties of SnS flakes through angle-resolved polarized Raman spectroscopy (ARPRS). It is found that the different Raman modes of SnS show distinctly anisotropic dependence on the thickness of flake. Specially, for B_{3g} mode, the polar plots of Raman intensities for both parallel and perpendicular polarization configurations are insensitive to the flake thickness. On the contrary, the behavior of A_g mode is

[a]Hefei National Laboratory for Physical Sciences at the Microscale, Department of Physics, University of Science and Technology of China, Hefei, Anhui 230026, P. R. China. E-mail: xpwang@ustc.edu.cn

[b]Synergetic Innovation Center of Quantum Information & Quantum Physics, University of Science and Technology of China, Hefei, Anhui 230026, P. R. China

[c]Key Laboratory of Strongly-Coupled Quantum Matter Physics, Chinese Academy of Sciences, School of Physical Sciences, University of Science and Technology of China, Hefei, Anhui 230026, P. R. China

† Electronic supplementary information (ESI) available: AFM image of 13.2 nm SnS flake, polar plots of B_{3g} (164.0 cm^{-1}) and A_g (95.9 cm^{-1} and 192.0 cm^{-1}) with different thickness, the calculated polar plots of A_g (||) mode with different $|C|/|B|$ and φ_{CB}, and variation of φ_{CB} with the thickness of SnS flake for A_g mode (192.0 cm^{-1}). See DOI: 10.1039/c7ra09430b

entirely different. For the parallel polarization configuration, with decreasing the flake thickness, the maximum of Raman intensity changes from the armchair direction to the zigzag direction under 514.5 nm excitation. The result can be interpreted by introducing complex Raman tensor caused by the large absorption.[33–36,38] Furthermore, the Raman intensity along 45° direction becomes different from that along 135° direction under the perpendicular polarization configuration. Our finding enriches the understanding of fundamental anisotropic Raman properties of SnS and implies the necessity to consider the thickness of SnS flake to identify its crystalline orientation through Raman characterization.

Experiments

Synthesis of 2D SnS flakes

The SnS flakes with different thicknesses were synthesized by physical vapor deposition (PVD) method.[25] The SnS powders (~0.1 g Alfa Aesar 99.5%) placed in the quartz tube were put onto the center of a horizontal furnace, and the freshly cleaved mica substrates were placed at 15–21 cm downstream. The furnace was evacuated to about 8 mTorr and was then purged with ultrapure Ar. The temperature of the furnace center is set at 630–650 °C. The pressure and the Ar flow were kept at ~29 Torr and 60 sccm during the growth, respectively. The SnS vapor was carried by Ar flow and deposited onto the substrates, and the SnS flakes were formed subsequently. The growth was maintained for 5–15 min. Then the furnace was cooled down immediately by opening the furnace.

Transfer method

The SnS flakes were transferred from mica to SiO$_2$/Si substrate by a water ultrasonic method. The flakes on mica were spin-coated with PMMA (A4 495) at 3000 rpm for 45 s, and then were put onto a hot plate and kept at 120 °C for 3 min. The PMMA film were separated from the mica substrate through dipping it into water and by ultrasonic for several minutes. After that, PMMA containing flakes was transferred onto SiO$_2$/Si substrate and gently dried with lamp heating. Finally, PMMA was removed by dipping in ethyl acetate and acetone, respectively.

TEM characterization

TEM, HRTEM images and SAED patterns were collected by a FEI Talos transmission electron microscope operated at 200 kV. The samples for characterization were transferred onto copper grids by the same method described above.

Raman measurement

The Raman spectra were obtained by LabRAM HR 800 Raman system under 514.5 nm and 632.8 nm excitation, respectively. The intensities on the samples for both 514.5 nm and 632.8 nm laser in our experiment are controlled at about 0.5 mW (0.4 mW) without (with) a polarizer in the exciting light path. We used 100× objective lens (N.A. = 0.9) and 600 lines per mm grating to collect Raman signals. The spectrum resolutions for

514.5 nm and 632.8 nm excitation are 1.88 cm^{-1} and 1.21 cm^{-1}, respectively. In polarization-dependent Raman measurement, a polarizer was placed in the incident light path to improve the polarization of exciting light and weaken the depolarization effects caused by objective lens. The direction of polarizer is fixed and the direction of analyzer is alterable. Two configurations of parallel (∥) and perpendicular (⊥) polarization were adopted in the measurement, in which the polarization direction of the polarizer and the analyzer were kept parallel or perpendicular to each other, respectively. The polarization direction of exciting laser with respect to the sample was changed by rotating a custom sample stage by every 5/10/15 degrees. The position and spot area of excitation were cautiously kept the same for each measurement.

Results and discussion

Fig. 1a shows the optical image of a typical result of as-grown SnS flakes. As seen, all flakes have square-like morphologies and their averaged size can reach as large as 10 μm, which can be observed more clearly in Fig. 1b. Atomic force microscopy (AFM) (Seiko Instrument Industry Co.) characterization demonstrates that the flake has a smooth surface morphology and its thickness can be down to 7.6 nm, as seen in Fig. 1c. The bright particles on the flake surface are the residues from the transfer process (see Fig. S1 in ESI†). We also note that the morphology of 7.6 nm SnS flake shows rounded corners, while most of flakes shown in Fig. 1a demonstrate sharp corners. Considering that the perfect rhombus structure with sharp
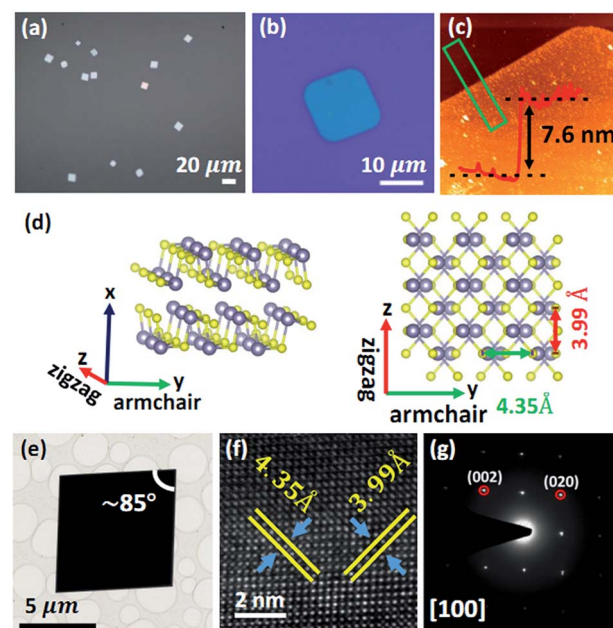

Fig. 1 (a) Optical image of as-grown SnS flakes on mica substrate and (b) a thin SnS flake transferred onto SiO$_2$/Si substrate. (c) AFM image of 7.6 nm thick SnS flake. (d) Schematic of crystal structure of SnS from side view (left) and top view (right). (e) TEM image of a SnS flake with a corner angle of ~85°. (f) HRTEM image and (g) SAED pattern of SnS flake.

corners is the thermodynamic equilibrium state of SnS flake[20] and the growth time for the thin flakes is much short (<5 min), we think that there might be no enough time to reach the thermodynamic equilibrium for the thin flakes, resulting in their rounded corners morphology. Additionally, we found that it is difficult to obtain the very thin flakes, because SnS has a relatively strong interlayer interaction[5,39] and the complicated phases of S and Sn compounds.[40]

We carried out transmission electron microscopy (TEM) as well as the selected area electron diffraction (SAED) characterizations to investigate the structure of the SnS flake and evaluate its crystal quality. Fig. 1d depicts the schematic of crystal structure of SnS. Similar to BP, SnS has also a puckered honeycomb structure, and the two in-plane principle axes are corresponding to armchair direction (y axis) and zigzag direction (z axis), respectively. As seen in Fig. 1e, the SnS flake transferred onto the TEM grids shows a rhombus shape, and the corner angle is estimated to ~85°, which is in good agreement with previous reports.[20,25] Additionally, the perfect 2D rhombus lattice can be found in the high resolution TEM image taken from the flake (Fig. 1f). Two lattice spacings corresponding to the (010) and (001) planes are obtained to be about 4.35 Å and 3.99 Å, respectively. The values are well consistent with the previous results.[20,25,41] Fig. 1g demonstrates the corresponding SAED pattern along [100] zone axis of the flake, and the well-defined diffraction spots reveal the good crystalline of as-grown SnS flake. It has been pointed out that the crystalline direction of the SnS can be readily identified from the rhombus shape, *i.e.*, the longer (shorter) diagonal direction is corresponding to the armchair (zigzag) direction.[20,25] Therefore, the method is used to ascertain the armchair (or zigzag) direction of the flake for the anisotropic characterization of Raman spectroscopy in the following paragraphs.

The flakes were characterized by the Raman spectroscopy with 514.5 nm laser and the spectra of flakes with different thicknesses are shown in Fig. 2a. As seen, for the thick flakes (169.0 nm and 229 nm), six peaks located at 40.2 cm^{-1}, 49.1 cm^{-1}, 95.9 cm^{-1}, 164.0 cm^{-1}, 192.0 cm^{-1} and 219.5 cm^{-1}

can be observed clearly. (The Raman peak positions are obtained from fitting the spectrum and its uncertainty is about 0.3 cm^{-1}). These peaks can be attributed to the different Raman modes of A_g and B_{3g} of SnS, respectively,[41] as shown in the schematic of Fig. 2b. Specifically, the low frequency A_g (40.2 cm^{-1}) and high frequency A_g (219.5 cm^{-1}) are corresponding to the layer shear mode and the "NaCl" type vibration, respectively. Two other A_g peaks (95.9 cm^{-1}, 192.0 cm^{-1}) are originated from the "waving" and the "breathing" modes, while B_{3g} (49.1 cm^{-1}) and B_{3g} (164.0 cm^{-1}) can be attributed to the shear vibration and the "NaCl" type vibration along zigzag direction, respectively.[41] From Fig. 2a, a little red shift of Raman peaks can be observed with decreasing the flake thickness. Taking 7.6 nm thick SnS as an example, the positions of three strong peaks are located at about 93.9 cm^{-1} (A_g^1), 151.7 cm^{-1} (B_{3g}) and 183.2 cm^{-1} (A_g^2), respectively. Compared to the results of 229 nm flake, the red shifts can be estimated about 2.0 cm^{-1} (A_g^1 mode), 12.3 cm^{-1} (B_{3g} mode) and 8.8 cm^{-1} (A_g^2 mode), respectively. The phenomenon might be ascribed to the change of bond angle in the thin flake, leading to the smaller of the restoring force for the vibration and the red shift of the corresponding Raman peak.[7]

To further investigate the anisotropic Raman response of SnS, the polarization-dependent Raman spectroscopy was performed on the SnS flake. As seen in Fig. 3a, the Raman spectrum was collected through the back-scattering configuration with a polarizer and an analyzer placed in the incident and the scattering light paths, respectively. Two configurations of parallel (∥) and perpendicular (⊥) polarization were adopted in the measurement, in which the polarization direction of the polarizer and the analyzer were kept parallel or perpendicular to each other, respectively (Fig. 3a). The polarization angle, defined as the angle between the polarization direction of incident light and the armchair direction of SnS flake, can be tuned from 0° to 360° through rotating a custom sample stage.

Fig. 3b and c demonstrate the anisotropic Raman response of 229 nm SnS flake to the different polarization angles with 514.5 nm excitation under parallel and perpendicular polarization configurations, respectively. As shown in Fig. 3b, A_g (95.9 cm^{-1}), B_{3g} (164.0 cm^{-1}) and A_g (192.0 cm^{-1}) are three strong peaks among the Raman spectra, we therefore concentrate on these three peaks in the following investigation. It can be seen from Fig. 3b and c that the peak intensities of A_g and B_{3g} change periodically with the polarization angle, indicating the anisotropic Raman signals of the SnS flake. The behavior can be observed more clearly with the polar plots for the modes of A_g (192.0 cm^{-1}) and B_{3g} (164.0 cm^{-1}), as shown in Fig. 3d–g. As seen in Fig. 3d, the Raman intensity of A_g (192.0 cm^{-1}, ∥) along armchair is larger than that along zigzag direction. However, it is worth noting that the intensity of zigzag direction is the secondary maximum here, rather than the minimum as the previous works reported.[20,25] This implies that the complex Raman tensor should be considered to interpret the result as that treated for BP.[33–36,38] On the other hand, as for the modes of B_{3g} (164.0 cm^{-1}, ∥), the intensities along armchair direction and zigzag direction are smallest while the intensities along 45° (225°) and 135° (315°) are the largest (Fig. 3f).
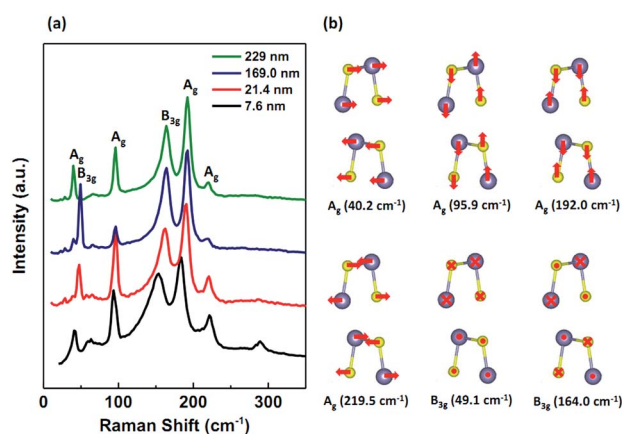

Fig. 2 (a) Raman spectra of SnS flakes with different thicknesses under 514.5 nm laser excitation. (b) Vibration diagrams for A_g modes and B_{3g} modes.
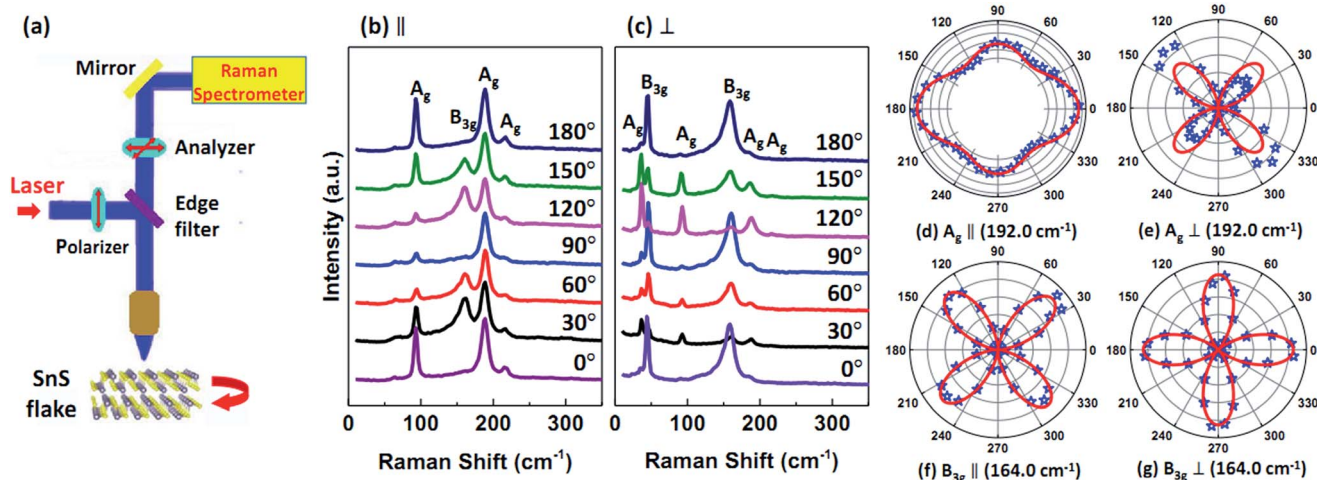
Fig. 3 (a) Schematic diagram of Raman measurement for SnS flake. Polarization-dependent Raman spectra of 229 nm thick flake with 514.5 nm laser excitation under (b) parallel and (c) perpendicular polarization configurations. (d–g) The polar plots of intensity of A_g (192 cm^{-1}) and B_{3g} (164.0 cm^{-1}) under parallel and perpendicular polarization, respectively.

Theoretically, the Raman intensity can be calculated by $I \propto |\mathbf{e_i} \cdot \mathbf{R} \cdot \mathbf{e_s}|^2$ and the anisotropic behavior is ascribed to the Raman tensor $\mathbf{R}$, which is determined by the detailed crystal structure of material. Owing to its large absorption coefficient,[9,10] the Raman tensor elements of the SnS should be complex. Consequently, similar to the treatment for BP,[33–36,38] the Raman tensors for A_g and B_{3g} of SnS can be described by

$$\mathbf{R}(A_g) = \begin{pmatrix} |A|e^{i\varphi_A} & 0 & 0 \\ 0 & |B|e^{i\varphi_B} & 0 \\ 0 & 0 & |C|e^{i\varphi_C} \end{pmatrix}$$

$$\mathbf{R}(B_{3g}) = \begin{pmatrix} 0 & 0 & 0 \\ 0 & 0 & |F|e^{i\varphi_F} \\ 0 & |F|e^{i\varphi_F} & 0 \end{pmatrix}$$

For the polarization angle of θ, the incident light vector is $\mathbf{e_i} = (0, \cos\theta, \sin\theta)$, while the scattering light vector is $\mathbf{e_s} = (0, \cos\theta, \sin\theta)$ for parallel polarization but $\mathbf{e_s} = (0, -\sin\theta, \cos\theta)$ for the perpendicular case. Hence, the anisotropic Raman intensities for different modes can be expressed as:

$$I(A_g, \parallel) \propto |B|^2 \cos^4\theta + |C|^2 \sin^4\theta + 2|B||C|\cos^2\theta\sin^2\theta\cos\varphi_{CB} \tag{1}$$

$$I(B_{3g}, \parallel) \propto |F|^2 \sin^2 2\theta \tag{2}$$

$$I(A_g, \perp) \propto \frac{|B|^2 + |C|^2 - 2|B||C|\cos\varphi_{CB}}{4}\sin^2 2\theta \tag{3}$$

$$I(B_{3g}, \perp) \propto |F|^2 \cos^2 2\theta \tag{4}$$

where $\varphi_{CB} = |\varphi_C - \varphi_B|$ is the phase difference between Raman tensor elements $|B|e^{i\varphi_B}$ and $|C|e^{i\varphi_C}$.

We fitted the experiment data with above equations, and the results are plotted in Fig. 3d–g with red solid lines. As seen, the fitting is well consistent with the experiment results. Moreover,

combined with the theory and experiment setup, the anisotropic behavior of A_g (192.0 cm^{-1}) mode can be understood from the fact that its vibration motion has more component in armchair direction than that in zigzag direction.[33–36,38] As for the mode of B_{3g} (164.0 cm^{-1}), there only exist off-diagonally non-zero elements in the Raman tensor. Therefore, when the polarization of incident light is along armchair (zigzag) direction, the polarization of Raman scattering light will switch to zigzag (armchair) direction. This leads to the intensities of B_{3g} (164.0 cm^{-1}) along armchair and zigzag directions become zero under the parallel polarization configuration (Fig. 3f) but achieve the maximum under the perpendicular polarization configuration, as shown in Fig. 3g.

In order to know whether the anisotropic Raman properties are dependent on the flake thickness, we carried out polarization-dependent Raman measurements on the SnS flakes with different thicknesses. Fig. 4a and b show the results for B_{3g} (164.0 cm^{-1}) under parallel and perpendicular polarization configurations, respectively. As seen, for both configurations, the polar plots of Raman intensity for different thick SnS flakes are similar to those shown in Fig. 3f and g, indicating that the B_{3g} mode is insensitive to the flake thickness. Similar results with 632.8 nm excitation are presented in Fig. S2.† The behavior can be easily understood by the description of eqn (2) and (4). However, as compared to B_{3g} mode, the situation of A_g mode is distinctly different. As seen in the Fig. 4c for the mode of A_g (192.0 cm^{-1}, $\parallel$), the Raman intensity along the armchair direction is larger than that along the zigzag direction for the thick flakes, but the behavior reverses for the thin flake, i.e., the Raman intensity along the zigzag direction becomes larger. This unusual result indicates that the anisotropic Raman response of SnS is strongly dependent on the flake thickness.

As indicated in the aforementioned paragraph, the intensity of A_g mode under parallel polarization configuration can be described by eqn (1), from which we can find that the polar plot of Raman intensity is determined by three parameters, $|C|$, $|B|$
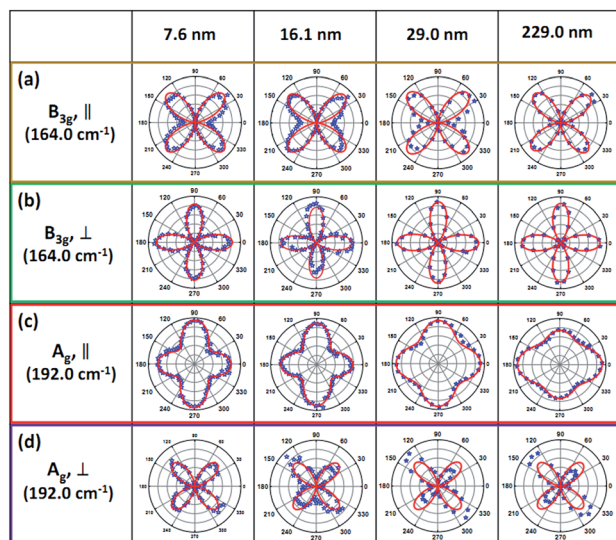
Fig. 4 Polar plots of Raman intensities of B_{3g} (164.0 cm^{-1}) and A_g (192.0 cm^{-1}) for different thick SnS flakes with 514.5 nm laser excitation under parallel and perpendicular polarization configurations, respectively. The red curves are fitting results.

and φ_{CB}. Several calculated results based on eqn (1) are shown in Fig. S3.† Obviously, $|C|^2/|B|^2$ is equal to the intensity ratio of the zigzag direction to the armchair direction, reflecting the Raman anisotropy in the y–z plane, while φ_{CB} determines the concave degree of the intensity pattern along nearby 45° (or 225°) and 135° (or 315°). Compared to the calculated pattern shown in Fig. S3,† the result in Fig. 4c therefore demonstrates that the ratio of $|C|^2/|B|^2$ varies with the thickness of SnS flake. The finding is important because it suggests that it is impossible to identify the armchair direction of SnS flake only through the maximum of Raman intensity, as that used previously.[20,25] Moreover, this variation tendency that the Raman intensity along zigzag direction increases with decreasing the flake thickness can also be observed with 632.8 nm excitation (Fig. S4d†).
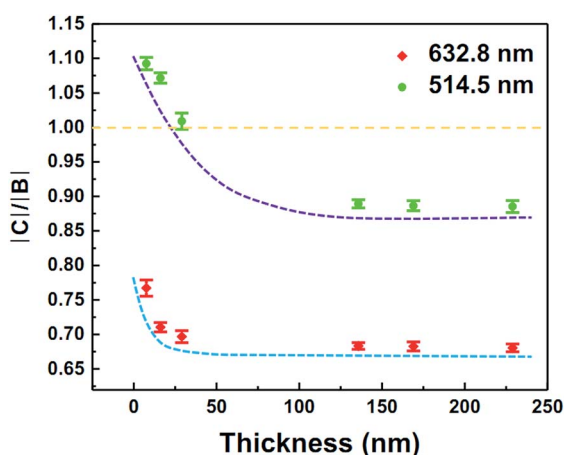

Fig. 5 Variation of $|C|/|B|$ with the thickness of SnS flake for A_g mode (192.0 cm^{-1}) with 514.5 nm and 632.8 nm laser excitation, respectively. The lines are guides for eye.

We used eqn (1) to fit the results of Fig. 4c and S4d,† and the fitting parameters $|C|/|B|$ and φ_{CB} are summarized in Fig. 5 and S5,† respectively. As seen in Fig. 5, two features can be found clearly. Firstly, for both 514.5 nm and 632.8 nm excitations, the value of $|C|/|B|$ decreases quickly with increasing the flake thickness and then reaches steady value for fairly thick flakes. The variation of φ_{CB} on the flake thickness has similar tendency (Fig. S5†). According to the semi-classical Raman theory, Raman tensor elements $|\mathbf{B}|e^{i\varphi_B}$ and $|\mathbf{C}|e^{i\varphi_C}$ are the partial derivatives of the dielectric constant of SnS with respect to the normal coordinates of the corresponding phonon modes along yy and zz directions, respectively.[33,38,42] In this context, we consider that the variation of $|C|/|B|$ with the flake thickness is probably attributed to the change of dielectric property for thin SnS flake as compared to that of the bulk. More importantly, Fig. 5 demonstrates $|C| > |B|$ for thin SnS flakes under 514.5 nm excitation, which is distinctly unusual as compared to the previous reports.[20,25] We ascribe the underlying reason to the strongly resonant absorption in zigzag direction for thin flake,[43] leading to the change of the dielectric dispersion relationship and hence the Raman tensor. More investigation is surely needed to elucidate this conjecture in the future work. Secondly, the values of $|C|/|B|$ with 514.5 nm excitation are larger than those with 632.8 nm excitation for all different thick flakes. The behavior can be further observed clearly by comparing Fig. 4c and S4d.† Because $|C|/|B| = 1$ is the indicative of Raman isotropy along armchair and zigzag directions, the result in Fig. 5 suggests that the anisotropic Raman spectrum can be observed more readily with 632.8 nm excitation.

Finally, we return to the anisotropic properties of A_g (192.0 cm^{-1}, ⊥) of SnS flakes with different thicknesses. As seen in Fig. 4d, all polar plots show the maximum values of Raman intensities along 45° (or 225°) and 135° (or 315°), while the minimum intensities are along armchair and zigzag directions. This is ascribed to that all non-diagonal elements in the Raman tensor of A_g modes are zero. As a consequence, when the polarization of excitation light is along armchair or zigzag direction, the final intensity of Raman scattering will become zero under perpendicular polarization configuration. Also from the prediction of eqn (2), the Raman intensity along 45° (or 225°) direction must be equal to that along 135° (or 315°) for A_g (⊥) mode. However, this contrasts obviously to the experimental observation for A_g mode (192.0 cm^{-1}, ⊥) shown in Fig. 4d, in which the intensity difference between 45° (225°) and 135° (315°) is apparent for the SnS flakes, especially for 29.0 nm and 229 nm flakes. The behavior has also been reported in SnS.[25] It is difficult to understand this phenomenon at present due to the fact that the 45° (or 225°) and 135° (or 315°) directions are equal from the viewpoint of crystal structure. One possible reason is attributed to the circular dichroism originated from the uniquely puckered anisotropic structure of SnS, leading to the different absorption along 45° and 135° directions.

Conclusions

We have successfully synthesized SnS flakes with different thicknesses by physical vapor deposition method. The anisotropy and the thickness dependence of Raman properties are

systematically investigated through the polarization-dependent Raman spectra. Both B_{3g} and A_g modes can be observed from the SnS flakes but they show distinctly anisotropic thickness dependence. On the one hand, the anisotropy of B_{3g} mode is found to be independent of the flake thickness. On the other hand, the A_g mode shows entirely different behavior. Under parallel polarization configuration and 514.5 nm excitation, the maximum Raman intensity of A_g mode changes from the armchair direction to the zigzag direction with decreasing the flake thickness. The result is interpreted through the complex Raman tensor due to the large absorption of SnS. Under the perpendicular polarization configuration, the Raman intensity of A_g mode along 45° direction becomes different from that along 135° direction. Our finding also implies that the anisotropic electron–phonon interactions in SnS flakes are dependent on the thickness. This work can enrich the understanding of fundamental anisotropic Raman properties of SnS and provide the inspiration for further studies on other 2D anisotropic materials.

Conflicts of interest

There are no conflicts of interest to declare.

Acknowledgements

Notes and references

1 J. R. Brent, D. J. Lewis, T. Lorenz, E. A. Lewis, N. Savjani, S. J. Haigh, G. Seifert, B. Derby and P. O'Brien, *J. Am. Chem. Soc.*, 2015, **137**, 12689.

2 V. Steinmann, R. Jaramillo, K. Hartman, R. Chakraborty, R. E. Brandt, J. R. Poindexter, Y. S. Lee, L. Sun, A. Polizzotti, H. H. Park and R. G. Gordon, *Adv. Mater.*, 2014, **26**, 7488.

3 L. C. Gomes and A. Carvalho, *Phys. Rev. B: Condens. Matter Mater. Phys.*, 2015, **92**, 085406.

4 M. Patel, A. Chavda, I. Mukhopadhyay, J. Kim and A. Ray, *Nanoscale*, 2016, **8**, 2293.

5 D. I. Bletskan, M. M. Bletskan and K. E. Glukhov, *J. Solid State Chem.*, 2017, **245**, 34.

6 P. Sinsermsuksakul, K. Hartman, S. B. Kim, J. Heo, L. Sun, H. H. Park, R. Chakraborty, T. Buonassisi and R. G. Gordon, *Appl. Phys. Lett.*, 2013, **102**, 053901.

7 C. Xin, J. X. Zheng, Y. T. Su, S. K. Li, B. K. Zhang, Y. C. Feng and F. Pan, *J. Phys. Chem. C*, 2016, **120**, 22663.

8 K. T. R. Reddy, N. K. Reddy and R. W. Miles, *Sol. Energy Mater. Sol. Cells*, 2006, **90**, 3041.

9 R. Eymard and A. Otto, *Phys. Rev. B: Solid State*, 1977, **16**, 1616.

10 L. Makinistian and E. A. Albanesi, *Phys. Status Solidi B*, 2009, **246**, 183.

11 B. Ghosh, M. Das, P. Banerjee and S. Das, *Semicond. Sci. Technol.*, 2009, **24**, 025024.

12 K. T. Ramakrishna Reddy, N. Koteswara Reddy and R. W. Miles, *Sol. Energy Mater. Sol. Cells*, 2006, **90**, 3041.

13 C. Xia, J. Du, W. Xiong, Y. Jia, Z. Wei and J. Li, *J. Mater. Chem. A*, 2017, **5**, 13400.

14 M. Patel, H. S. Kim and J. Kim, *Nanoscale*, 2017, DOI: 10.1039/c7nr03370b.

15 M. Ristov, G. Sinadinovski, M. Mitreski and M. Ristova, *Sol. Energy Mater. Sol. Cells*, 2001, **69**, 17.

16 X. Zhou, L. Gan, Q. Zhang, X. Xiong, H. Li, Z. Zhong, J. Han and T. Zhai, *J. Mater. Chem. C*, 2016, **4**, 2111.

17 T. Rath, L. Gury, I. Sanchez-Molina, L. Martinez and S. A. Haque, *Chem. Commun.*, 2015, **51**, 10198.

18 F. Lu, J. Yang, R. Li, N. Huo, Y. Li, Z. Wei and J. Li, *J. Mater. Chem. C*, 2015, **3**, 1397.

19 S. Sucharitakul, U. R. Kumar, R. Sankar, F. C. Chou, Y. T. Chen, C. H. Wang, C. He, R. He and X. P. A. Gao, *Nanoscale*, 2016, **8**, 19050.

20 Z. Tian, C. L. Guo, M. X. Zhao, R. R. Li and J. M. Xue, *ACS Nano*, 2017, **11**, 2219.

21 R. Guo, X. Wang, Y. Kuang and B. Huang, *Phys. Rev. B: Condens. Matter Mater. Phys.*, 2015, **92**, 115202.

22 Asfandiyar, T. R. Wei, Z. Li, F. H. Sun, Y. Pan, C. F. Wu, M. U. Farooq, H. Tang, F. Li, B. Li and J. F. Li, *Sci. Rep.*, 2017, **7**, 43262.

23 L. Medrano Sandonas, D. Teich, R. Gutierrez, T. Lorenz, A. Pecchia, G. Seifert and G. Cuniberti, *J. Phys. Chem. C*, 2016, **120**, 18841.

24 R. Fei, W. Li, J. Li and L. Yang, *Appl. Phys. Lett.*, 2015, **107**, 173104.

25 J. Xia, X. Z. Li, X. Huang, N. N. Mao, D. D. Zhu, L. Wang, H. Xu and X. M. Meng, *Nanoscale*, 2016, **8**, 2063.

26 R. E. Banai, L. A. Burton, S. G. Choi, F. Hofherr, T. Sorgenfrei, A. Walsh, B. To, A. Cröll and J. R. S. Brownson, *J. Appl. Phys.*, 2014, **116**, 013511.

27 J. Xia, D. Zhu, X. Li, L. Wang, L. Tian, J. Li, J. Wang, X. Huang and X.-M. Meng, *Adv. Funct. Mater.*, 2016, **26**, 4673.

28 Z. Zhang, J. Yang, K. Zhang, S. Chen, F. Mei and G. Shen, *J. Mater. Chem. C*, 2017, DOI: 10.1039/c7tc02865b.

29 C. J. Murphy, T. K. Sau, A. M. Gole, C. J. Orendorff, J. Gao, L. Gou, S. E. Hunyadi and T. Li, *J. Phys. Chem. B*, 2005, **109**, 13857.

30 S. D. Hudson and G. Chumanov, *J. Phys. Chem. C*, 2008, **112**, 19866.

31 J. Wu, N. Mao, L. Xie, H. Xu and J. Zhang, *Angew. Chem,. Int. Ed.*, 2015, **54**, 2366.

32 X. Wang, A. M. Jones, K. L. Seyler, V. Tran, Y. Jia, H. Zhao, H. Wang, L. Yang, X. Xu and F. Xia, *Nat. Nanotechnol.*, 2015, **10**, 517.

33 H. B. Ribeiro, M. A. Pimenta, C. J. S. de Matos, R. L. Moreira, A. S. Rodin, J. D. Zapata, E. A. T. de Souza and A. H. C. Neto, *ACS Nano*, 2015, **9**, 4270.

34 J. Kim, J. U. Lee, J. Lee, H. J. Park, Z. Lee, C. Lee and H. Cheong, *Nanoscale*, 2015, **7**, 18708.

35 X. Ling, S. Huang, E. H. Hasdeo, L. Liang, W. M. Parkin, Y. Tatsumi, A. R. Nugraha, A. A. Puretzky, P. M. Das, B. G. Sumpter, D. B. Geohegan, J. Kong, R. Saito, M. Drndic, V. Meunier and M. S. Dresselhaus, *Nano Lett.*, 2016, **16**, 2260.

36 A.-L. Phaneuf-L'Heureux, A. Favron, J.-F. Germain, P. Lavoie, P. Desjardins, R. Leonelli, R. Martel and S. Francoeur, *Nano Lett.*, 2016, **16**, 7761.

37 W. Lu, X. Ma, Z. Fei, J. Zhou, Z. Zhang, C. Jin and Z. Zhang, *Appl. Phys. Lett.*, 2015, **107**, 021906.

38 W. Luo, Q. Song, G. Zhou, D. Tuschel and G. Xia, arXiv, 1610.03382, 2016.

39 P. M. NikoliC, L. j. Iljkovic, P. Mihajlovic and B. LavrenEic, *J. Phys. C: Solid State Phys.*, 1977, **10**, L289.

40 R. C. Sharma and Y. A. Chang, *J. Phase Equilib.*, 1986, **7**, 269.

41 H. R. Chandrasekhar, R. G. Humphreys, U. Zwick and M. Cardona, *Phys. Rev. B: Solid State*, 1977, **15**, 2177.

42 A. C. Albrecht, *J. Chem. Phys.*, 1961, **34**, 1476.

43 G. A. Tritsaris, B. D. Malone and E. Kaxiras, *J. Appl. Phys.*, 2013, **113**, 233507.